Materials Science-Poland, 40(2), 2022, pp. 223-239
http://www.materialsscience.pwr.wroc.pl/
DOI: 10.2478/msp-2022-0023

Electrical resistance and self-sensing properties of pressure-sensitive materials with graphite filler in Kuralon fiber concrete

An Cheng[1], Wei-Ting Lin[1,*], Lukáš Fiala[2], Petr Hotěk[2], Sao-Jeng Chao[1], Hui-Mi Hsu[1]

[1]Department of Civil Engineering, National ILan University, Yilan County 260, Taiwan

[2]Department of Materials Engineering and Chemistry, Faculty of Civil Engineering, Czech Technical University in Prague, Thákurova 2077/7, 166 29 Prague 6, Czech Republic

This study aimed to investigate conductivity behavior of concrete containing graphite and its sensitivity to the effects of pressure. Graphite powder was added to concrete to replace partial cement (4 wt.%, 8 wt.%, 12 wt.%, and 16 wt.%) as conductive fillers with a water-to-cementitious ratio of 0.45. Specimens with 0.5 vol.% Kuralon fibers were treated to enhance the performance of self-sensing properties to investigate the influence of graphite and fiber contents on electrical resistivities. The relationship between the axial load and changes in resistivity was determined using cyclic loading tests, indicating the existence and development of internal cracking in concrete. The results indicated that the compressive strength presented a linear decline proportional to the addition of graphite. Specimens with 8% graphite reached the lower bound of self-sensing properties, and with an increase in the amount of graphite, resistivity gradually decreased. In the cyclic loading tests, specimens containing >8% graphite were able to better reflect the relationship between loading and resistivity. Kuralon fibers in concrete had further improvement in resistance and self-sensing properties. In inclusion, the mixture with 8% graphite provided the best self-sensing properties to warn for preventing the effects of cracking, as well as achieved better mechanical properties.

Keywords: *pressure-sensitive materials, graphite powders, resistivity change rate, cyclic loading test*

1. Introduction

As time goes by, functional and material degradations in concrete structures tend to appear due to internal defects. For large structures such as buildings, bridges, and dams, internal cracks or defects within the material can cause sudden collapses, resulting in a significant loss of life and property. If such defects could be discovered automatically, warnings could be issued before tragedy strikes [1]. The prevention of these sudden incidents during material degradation has been the focus of material research [2]. In terms of concrete, researchers have worked toward developing smart concrete [3] based on the concept of conductive composites [4]. In addition to performing the original structural functions of concrete [5], smart concrete also offers the functions of self-diagnosis [6], self-repair [7], self-heating [8], and chloride removal [9].

Concrete is currently the most widely applied material in civil engineering due to its mechanical stability [10] and durability [11] and is easy to acquire. It is also versatile and has high compressive strength. As a result, its development has been extremely swift. However, its low ductility and poor resistance to tension, bending [12], and impact are disadvantages of concrete materials [13]. It has led to the development of fiber-reinforced concrete to enhance deformability [14], toughness, and ductility [15]. However, concrete has extremely high resistivity and no self-sensing or electrical conduction capacity. It is necessary to use conductive materials such as graphite, carbon fiber, metal wastes, and metal powders or fibers in concrete composites to attain self-diagnosis capabilities [16]. Such composites can be considered smart materials [17]. Integrating smart materials and components has become a significant development following composite and functional materials.

* E-mail: wtlin@niu.edu.tw

© An Cheng et al. 2022. This is an open access article distributed under the Creative Commons Attribution-NonCommercial-NoDerivatives 4.0 License. (http://creativecommons.org/licenses/by-nc-nd/4.0/)

Several studies have recently developed smart concrete containing carbon fibers [18], graphite [19], slag, or other conductive fillers as pressure-sensitive materials [20]. The smart materials can be used to develop a monitoring and predicting technology that can quickly assess the extent of structural degradation using the pressure-sensitive properties of smart materials, facilitating the development of smart building materials. By observing the macroscopic behavior and microscopic structures of materials, it was discovered that resistivity variations corresponded to internal structural deformation under uniaxial compressive load. For instance, reversible resistivity changes tallied with elastic deformations in the material structure, whereas irreversible resistivity changes were consistent with non-elastic structural deformations and even material failure. Accordingly, the fluctuations in the resistivity of concrete reinforced with carbon fiber can be used to determine whether the concrete is structurally safe or damaged. Also, the study investigated the influence of the curing period and surface treatments of carbon fiber on self-diagnosis behavior. The regularity of resistivity changes in carbon fiber-reinforced concrete under different loading conditions can be used to diagnose and monitor the internal stress and strain and health status of the concrete [21], weigh moving vehicles, and even monitor traffic [22]. Smart materials or concrete with pressure-sensitive properties have great potential in structural health monitoring [23].

Conductivity is an essential property for the self-diagnosis of a cement-based material. Increasing conductivity and magnifying the electric signals mean that electric instruments are not sensitive [24]. Most studies have investigated the resistance of self-sensing concrete using composite materials [25] and admixtures [26]. In addition, the age, degree of hydration [27], and moisture content [28] of cement matrix materials are critical factors in the influence of electrical resistance [29]. Hanxun et al. [30] showed that dried polyvinyl alcohol fiber specimens showed higher resistivity based on the effect of the moisture content on resistivity due to changes in electrical conductivity of the filler and the concrete matrix. Water in micropores acts as an electrolyte and conductive electrons, leading to a variation in the resistance of the specimen [29]. Using fine particles such as carbon black increased the pressure-sensitive response of the specimen [29]. At the same time, fine particles were also helpful in accelerating the hydration of the specimen and increasing the conductivity and self-sensing ability [31]. By contrast, construction and material costs are important considerations for future applications in the construction field. Fibers are the most common composite additives used to obtain good electrical conductivity [32] as they help form a conductive network within the concrete [33]. Composite additives that can enhance the conductivity of cement-based materials include graphite and fibers comprising steel or carbon. This study incorporated graphite into concrete and adopted the production method for Kuralon fiber concrete to produce graphite-infiltrated fiber cement-based materials, a smart material with high conductivity. The mechanical and electrical properties of graphite-infiltrated fiber concrete were investigated for pressure sensitivity.

2. Test materials and methods

2.1. Test materials

This study used Type I Portland cement from Taiwan Cement Corporation. The physical and chemical properties of this cement met the specifications of American Society for Testing and Materials (ASTM) C150. The content of CaO, SiO_2, and Al_2O_3 in cement was 68.0%, 20.7%, and 5.1%, respectively. The fine aggregate came from the Lanyang River, and its fineness modulus equaled 2.86. The retention percentages of fine aggregates in No. 8 sieve, No. 16 sieve, No. 32 sieve, No. 50 sieve, and No. 100 sieve were 25.4%, 21.3%, 13.7%, 10.3%, and 9.4%, respectively. The particle size distribution of the fine aggregate met the specifications of ASTM C33. The maximum size of coarse aggregate was 12.5 mm.

Graphite powders (C-B01-P3000-999) manufactured by Ceramet Inc. (Taipei, Taiwan) were used. The purity of the powders was >99.9% (carbon), and the particle size varied from 5 μm to

1 mm (D50 was 10 μm).

The Type G superplasticizer (a water-reducing ratio of 12%) produced by Poplar Company (Taipei, Taiwan) was used to enhance the fluidity of all mixtures. The electrodes used in this study comprised a double-sided conducted aluminum foil tape manufactured by Tai Puu Tape Company (Taipei, Taiwan). The width and surface resistivity of the tape are 2.5 cm and 0.05 Ω, respectively, and it displayed good adhesiveness with concrete specimens.

Kuralon (K) fiber is a new polyvinyl alcohol fiber manufactured by the Japanese company Kuraray. The diameter, length, and aspect ratio of fiber are 0.75 mm, 30 mm, and 40 mm, respectively (see Figure 1). Table 1 presents the basic properties of the fibers. The fibers bond well with cement substrates and are widely applied in industry and construction.

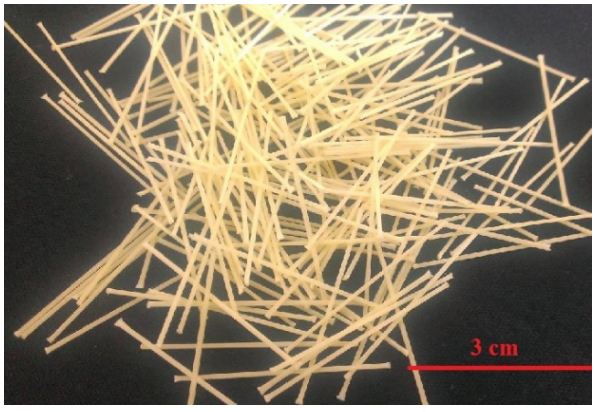


Fig. 1. Appearance of Kuralon fibers

Table 1. Properties of Kuralon fibers

Property	Testing value
Relative density	1.30
Tensile strength	880–1,600 MPa
Elongation	6%
Elastic modulus	29.12 GPa

2.2. Mixture proportions and tests conducted

Graphite powder was used to replace 0%, 4%, 8%, 12%, and 16% by weight of the cement in the concrete. The cementitious material was the sum of cement and graphite powders, and water included the superplasticizer. Considering that the inclusion of graphite reduces the strength of the concrete, we used a lower water-to-cementitious ratio of 0.45 so that the concrete would reach basic engineering strength requirements. We also compared mixtures containing an extra 0.5% of the total volume of K fibers with those not containing K fibers. Table 2 displays the various mixture proportions that we experimented to understand the differences between the properties of concrete with different graphite contents and whether adding fibers can enhance its performance. The addition of the superplasticizer was quantified by the weight of the cement. In addition, the graphite powder was taken in the mixer with the cement for mixing during the mixing process. The specimens were placed in water curing after demolding and taken out of the curing pool before the tests. The results of each test were averaged from three specimens, and the standard deviation was controlled to within 5%.

The first letters K and N in the mixture number distinguish the specimens with and without K fibers, referred to as fiber and normal concrete in this study. The second letter G stands for graphite, and the number behind G indicates the volumetric proportion of cement replaced with graphite powder. Thus, the graphite contents of 0%, 4%, 8%, 12%, and 16% are denoted as G0, G4, G8, G12, and G16, respectively. Table 3 shows the tests performed in this study. The test results of each test were averaged by using three specimens.

2.3. Method of resistivity measurement

The measurement of resistivity in concrete requires electrodes. Electrodes may be embedded or attached to the outside of the specimen. For the sake of costs and convenience in application, it used a conductive aluminum foil tape (width: 2.5 cm), which can be applied to the surface of specimens with a conductive adhesive. The standard resistivity measurement methods included the two-electrode and the four-electrode approaches. The latter can more effectively eliminate non-ohmic contact resistance than the former. For this

Table 2. Mixture designs of concrete (kg/m^3)

Mix No.	Water	Cement	Coarse aggregates	Fine aggregates	Graphite powders	K fibers	Superplasticizer
NG0	236.46	535.0	929.8	612.96	0	0	2.67
NG4	234.85	513.6	929.8	612.96	21.4	0	4.28
NG8	233.54	492.2	929.8	612.96	42.8	0	5.59
NG12	232.17	470.8	929.8	612.96	64.2	0	6.96
NG16	231.64	449.4	929.8	612.96	85.6	0	7.49
KG0	236.46	535.0	929.8	612.96	0	6.5	2.67
KG4	234.85	513.6	929.8	612.96	21.4	6.5	4.28
KG8	233.54	492.2	929.8	612.96	42.8	6.5	5.59
KG12	232.17	470.8	929.8	612.96	64.2	6.5	6.66
KG16	231.64	449.4	929.8	612.96	85.6	6.5	7.49

Table 3. Concrete tests

Specimen	Properties	Detailed tests	Standard
Concrete	Hardened concrete properties	Compressive strength test	ASTM C39
		Elastic modulus test	ASTM C469
		Flexural strength test	ASTM C78
	Permeability	Saturated absorption test	ASTM C642
		ISA test	BS 1881
	Microscopic properties	Scanning electron microscopy	ASTM C1723
	Electrical properties	Four-electrode resistivity test	Wenner method
		DC loop resistance test	Designed method in Section 2.3
		Cyclic loading test	

DC, direct current; ISA, initial surface absorption

reason, the four-electrode method was chosen to measure resistivity. In addition, the specimens kept were under saturated surface-dry conditions to avoid the influence of humidity on the resistance measurement of the specimen [29].

Figure 2 displays the schematics of resistivity measurement; we used a 7V DC power source and placed the specimen in a series with a resistor of known resistance. As the currents passing through, the specimen and the resistor are equal in magnitude according to Ohm's law, $\frac{V_1}{R_1} = \frac{V_2}{R_2}$ means that $R_1 = \frac{V_1}{V_2}R_2$, where R_1 and R_2 denote the resistance of the specimen and the resistor (a known resistance), respectively. After obtaining V_1 and V_2 using a data collector, we can observe the resistance variations in the specimens. Subsequently, the resistivity can be calculated using the formula $\rho = \frac{RA}{L}$, where ρ is the resistivity (kOhm-cm), R is the resistance of the specimen (Ohm), A denotes the cross-sectional area of the specimen (cm^2), and L symbolizes the distance (cm) between the two electrodes (V_1 and V_2). Figure 3 shows a photo of the actual experiment.

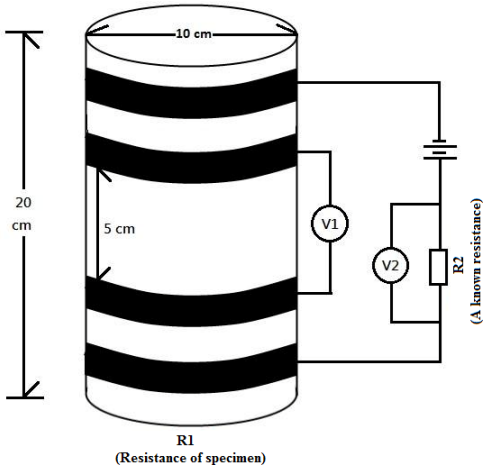


Fig. 2. Schematics of resistance measurement



Fig. 3. Appearance of actual resistance measurement

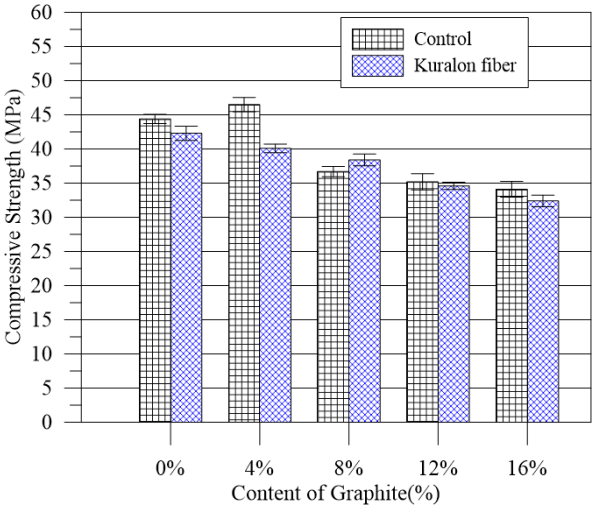


Fig. 4. Compressive strength of normal and fiber concrete groups at 56 days

3. Results and discussion

3.1. Compressive strength

Figure 4 displays the results of the compressive strength histograms. Except NG4, the normal concrete specimens without K fibers (NG series specimens) showed a decline in compressive strength as the graphite content increases. Comparing the strength reduction rates between the normal and fiber concrete specimens revealed that the fiber concrete specimens with a graphite content $<8\%$ presented significantly lower strength reduction rates than the normal concrete specimens with the same graphite content. By contrast, the strength reduction rates of the two types of concrete with graphite contents $>12\%$ were roughly the same. It was speculated that this may have been because the fibers generated a binding force in the specimens that counteracted the friction reduction caused by graphite [34]. The addition of graphite compound fibers enhanced the electrical conductivity of the concrete, but the excessive usage had a negative impact on the compressive strength [35]. However, once the graphite content reached 12%, the internal binding force could not rival the overly low friction, which increased the reduction in strength. It was concluded that the corresponding relationship between conductivity and strength must be considered when using graphite as a conductive material to produce conductive concrete.

3.2. Elastic modulus

The addition of graphite decreases the elastic modulus of the concrete specimens (see Figure 5). Among the normal concrete specimens, the elastic modulus of the specimen with 4% graphite content (specimen NG4) was not significantly different from that of the control specimens (specimen NG0). By contrast, those with 8%, 12%, and 16% graphite contents were lower by 11%–15%. The decrease is likely due to the directly proportional relationship between compressive strength and the elastic modulus (see Figure 6), which means that the elastic modulus declines when the compressive strength decreases. Among the fiber concrete specimens, the elastic modulus of those with 4% and 8% graphite contents was roughly 4% lower than that of specimen KG0. In comparison, the specimens with 12% and 16% graphite contents were lower by 9%–12%. A comparison of the normal and fiber concrete specimens showed that the elastic modulus of the specimens containing K fibers did not decrease as much, thereby indicating that K fibers can raise the upper limit of the linear stage of elastic modulus development.

Figure 6 compares the regression curve of the elastic modulus and compressive strength in this study with that in ACI 318; clearly, the regression curve of this study is considerably lower. This is

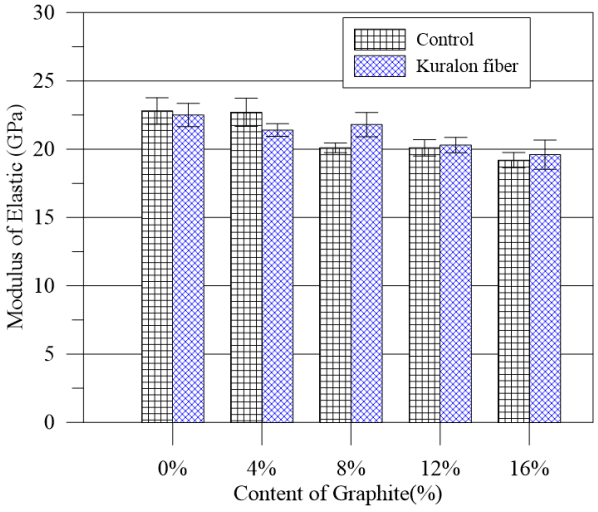


Fig. 5. Elastic modulus of concrete specimens at 56 days

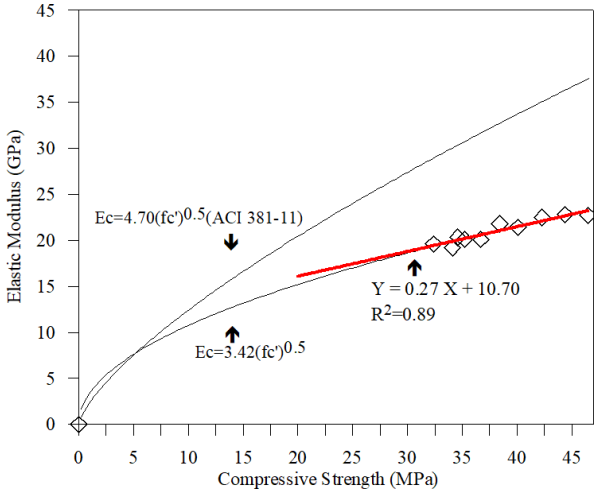


Fig. 6. Regression curves of compressive strength with regard to the elastic modulus

likely because the strength of foreign aggregate is higher than that in Taiwan cement, which reduces the aggregate-to-cement ratio in the cement and the elastic modulus.

3.3. Flexural strength

Figure 7 shows the results of the flexural strength test, in which the assessed index is the modulus of rupture. The normal concrete specimens presented declining flexural strength as the graphite content increased. The specimens with 8%, 12%, and 16% graphite contents displayed reductions of 8.8%, 12.4%, and 22.9%, respectively, compared with the control group. Only the specimen with a 4% graphite content had higher flexural strength than the control group, which may be because of its higher compressive strength.

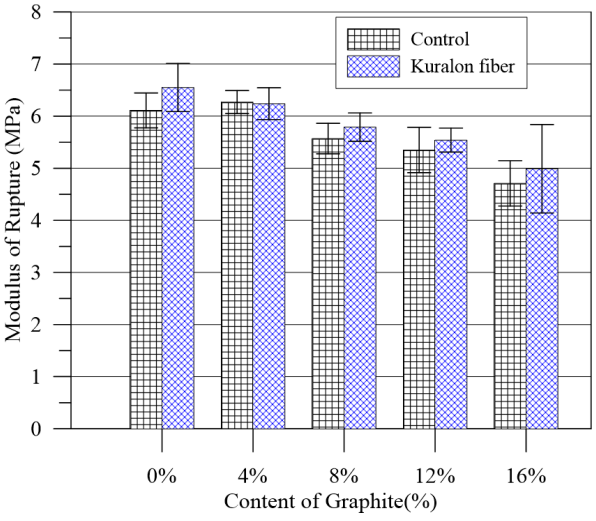


Fig. 7. Modulus of rupture of concrete specimens at 56 days

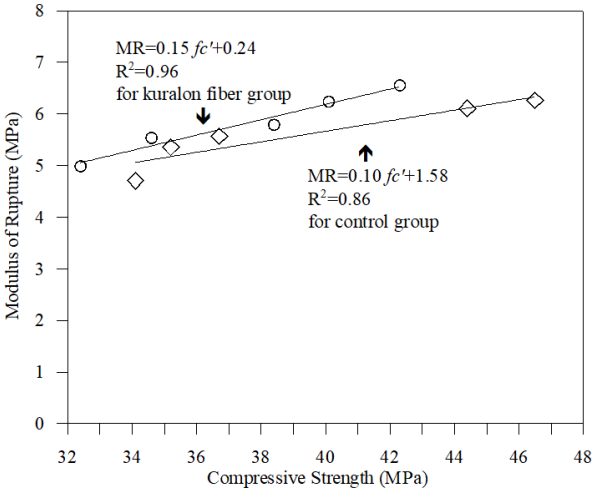


Fig. 8. Regression curves of compressive strength with regard to the modulus of rupture

Flexural strength also declined among the fiber concrete specimens as the graphite content increased. Regarding the magnitude of reduction in flexural strength, the specimen with a 4% graphite

content presented a reduction of approximately 4.7%. By contrast, the specimens with 8%, 12%, and 16% graphite contents displayed reductions of 11.6%, 15.4%, and 23.8%, respectively. A comparison of the normal and fiber concrete specimens, as presented in Figure 7, showed that the specimens containing K fibers possessed greater flexural strength than the normal concrete specimens. Figure 8 shows the regression curve of compressive strength concerning the modulus of rupture. As can be seen, the fiber concrete curve is slightly higher than the normal concrete curve, which means adding K fibers enhanced the flexural strength of the concrete specimens.

3.4. Saturated absorption rate

The saturated water absorption rate of concrete shows how the porosity and density of the concrete progress with time. Figure 9 displays the results of the saturated water absorption test. Except for NG4, the normal concrete specimens presented lower saturated water absorption rates than the control group. Furthermore, the saturated water absorption rate increased significantly with the graphite content. A comparison of the normal and fiber concrete specimens showed roughly the same saturated water absorption rates in both the groups, which indicates that K fibers cannot reduce the internal porosity of the concrete. The use of graphite powder to replace the amount of cement in the specimen would increase the internal porosity of the mortar, reducing the compactness of the concrete. The gradually increased water absorption and decreased compressive strength tests showed no significant hydration reaction between the graphite powders and the cement particles. Wang et al. [36] found that the specimens with functional fillers produced more hydration crystals than the control ones. Thus, accelerated hydration growth led to reduced porosity, better compactness, pore refinement [37], and an improved microstructure [38].

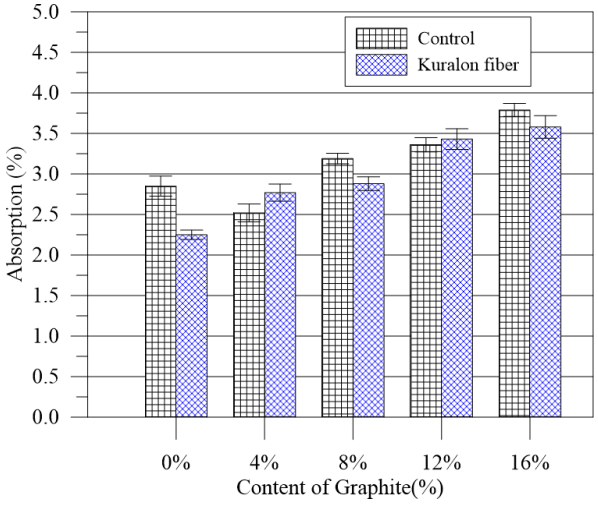


Fig. 9. Saturated water absorption rates of normal and fiber concrete specimens at 56 days

3.5. Initial surface absorption (ISA) rate

The ISA test assesses the capillary adsorption of outside water molecules in the pores of cement-based materials. According to the specifications of BS 1881, the ISA rate is defined as the amount of water absorbed by a fixed surface area of the cement-based material in contact with water within a specified period. This test was performed after a curing period of 56 days. We used the parameters established by Kumar and Bhattacharjee [39] to determine the permeability of the concrete specimens (see Table 4).

Table 4. Permeability of concrete [39]

Time (min)	**Permeability of concrete using ISA (ml/m^{2}s)**		
	Low	**Average**	**High**
10	<0.25	0.25-0.50	>0.50
30	<0.17	0.17-0.35	>0.35
60	<0.07	0.10-0.20	>0.20

ISA, initial surface absorption

As shown in the test results in Figures 10 and 11, all specimens showed high permeability at 30 s, except NG0, NG4, and KG0. Figure 10 indicates that surface water absorption rates increase with the graphite content. Greater surface water absorption rates result from higher porosity, causing the adhesive force of the water to the pore walls to be greater than the cohesive force within the water. It demonstrates that adding graphite increases the internal porosity of concrete. The results, as displayed in Figure 11, show the same trend among

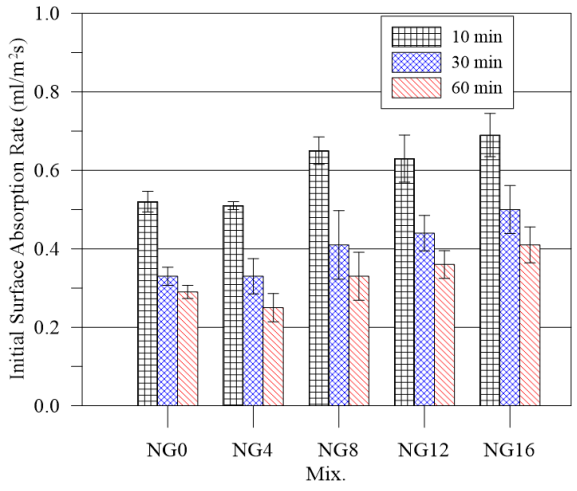


Fig. 10. Initial surface water absorptions rates of normal concrete specimens at 56 days

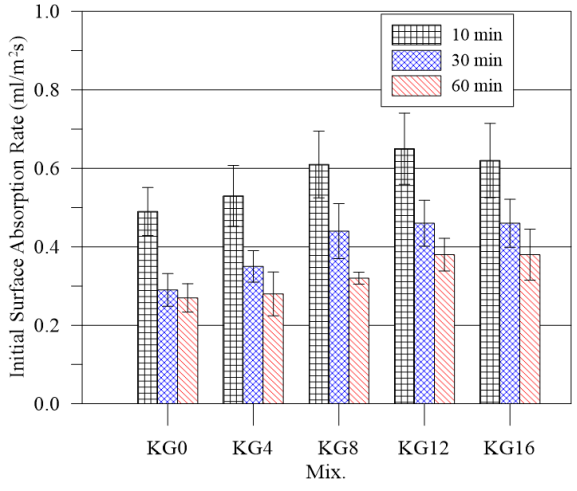


Fig. 11. Initial surface water absorptions rates of fiber concrete specimens at 56 days

the fiber concrete specimens. The lack of differing increases or decreases shows that adding K fibers does not significantly change the internal porosity of the concrete.

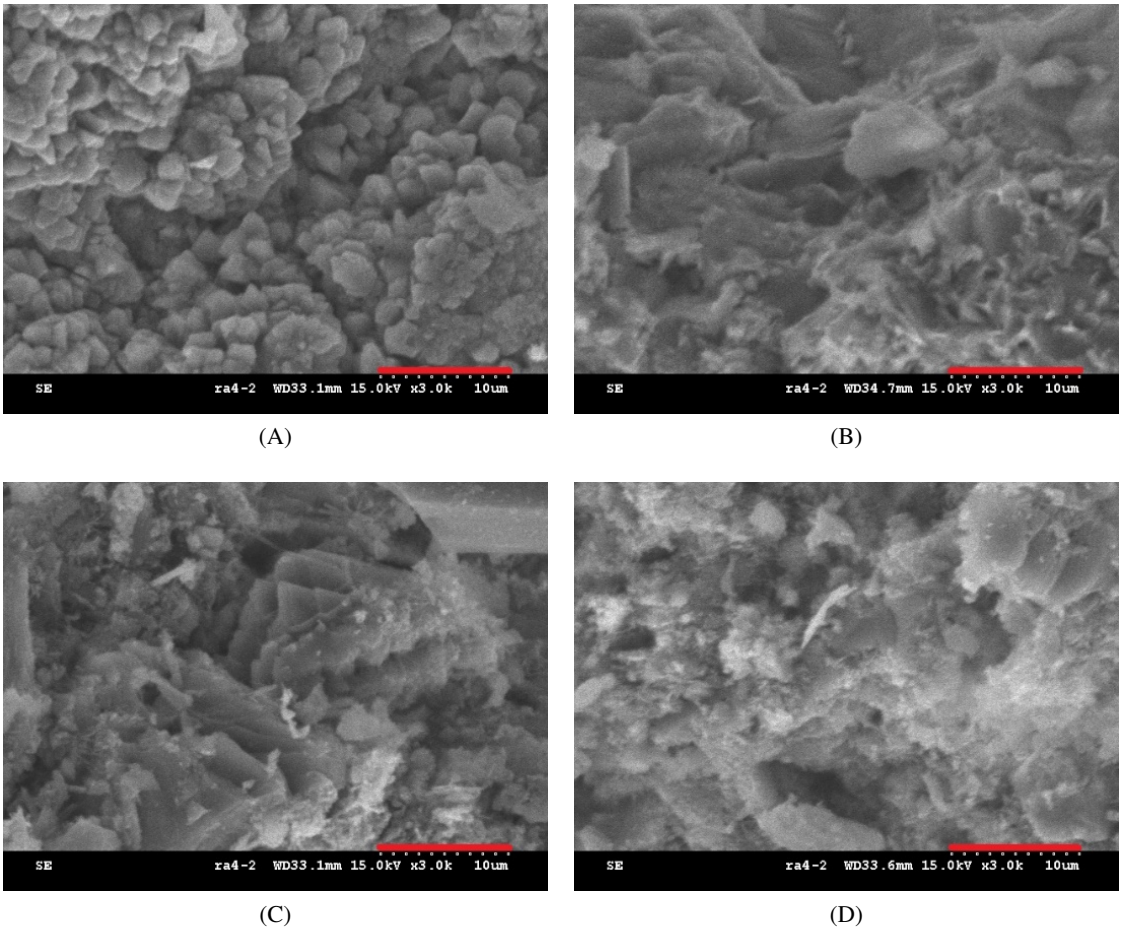
3.6. Scanning electron microscopy

Figure 12 presents the scanning electron microscopy (SEM) images of specimens (NG series specimens) with 0%, 4%, 8%, and 12% graphite (at a magnitude of 3,000 times). In terms of porosity, the images show that porosity increases with the graphite content. Comparing the three images containing graphite displays an even increasing distribution of graphite particles. The specimen with a 12% graphite content also presents graphite clusters. Graphite can evenly mix with the cement in specimens with a lower graphite content. However, as the graphite content increases, the quantity of water required increases, thereby preventing some particle clumps from dispersing. Furthermore, the surface of graphite particles has some magnetism, which causes some graphite particles to cluster when the graphite content is high.

3.7. Resistivity coefficient obtained using four-electrode method

Figures 13 and 14 show the resistivity coefficients of the concrete specimens derived using the four-electrode approach. As shown in Figure 13, the resistivity coefficients of the normal concrete specimens containing graphite show the same trend as the mortar [40], in which resistivity decreases as the graphite content increases. The specimen with a 4% graphite content presents approximately 7.4% lower resistivity than the control group, while the specimens with 8%, 12%, and 16% graphite contents show resistivity lower by 37.8%, 46.7%, and 47.4%, respectively. The resistivity coefficients of the fiber concrete specimens in Figure 14 show that the specimen with a 4% graphite content has approximately 14.4% lower resistivity, whereas the specimens with 8%, 12%, and 16% graphite contents show resistivity lower by 35.5%, 35.9%, and 43.2%, respectively.

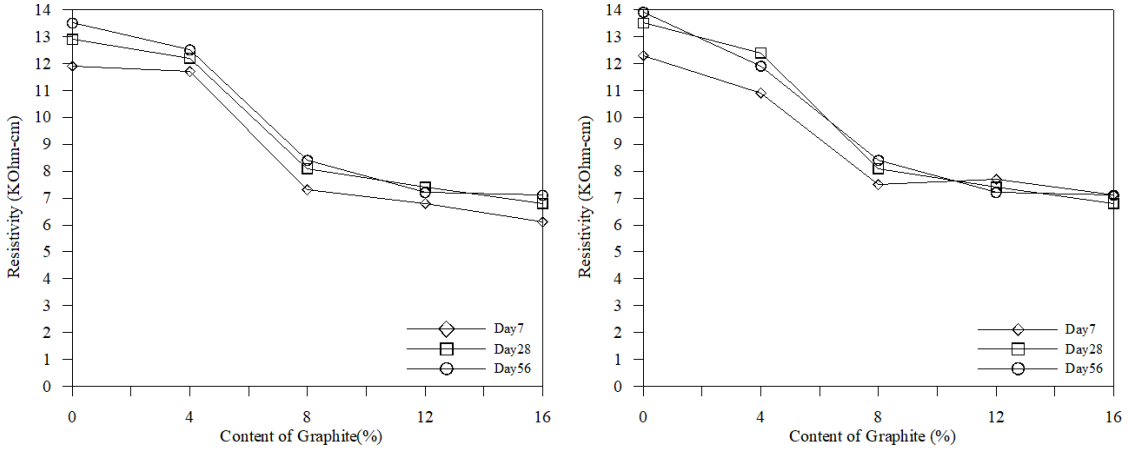
The results show that resistivity did not significantly decrease until the graphite content reached 8%, indicating a slight difference from that of the graphite content of 5%, corresponding to the percolation threshold of the mortar [22]. The cause of this difference may be because the media within the mortar [40] is evenly distributed with small particles, enabling the graphite to form conductive pathways within the specimens. By contrast, the concrete specimens contain coarse aggregates, consisting of larger particles and requiring electrons to travel longer paths than they would in a mortar. It caused the percolation threshold to increase to a graphite content of 8%.



(A) (B)

(C) (D)

Fig. 12. SEM image (3,000×). **(A)** NG0, **(B)** NG4, **(C)** NG8, and **(D)** NG12



(A) (B)

Fig. 13. Resistivity coefficients using the four-electrode method. **(A)** Normal concrete specimens and **(B)** Fiber concrete specimens

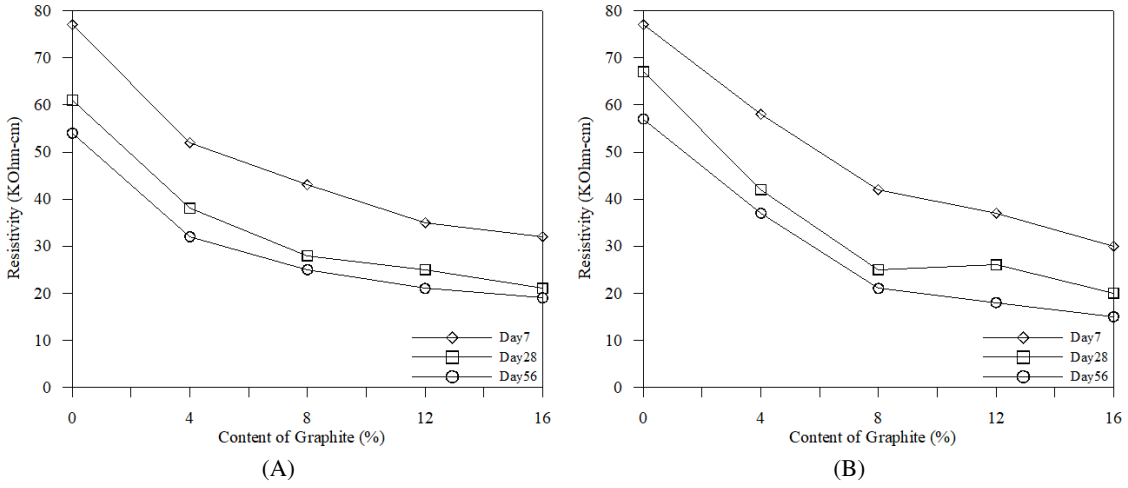


Fig. 14. Resistivity coefficients using the DC loop resistance test. **(A)** Normal concrete specimens and **(B)** Fiber concrete specimens. DC, direct current

The resistivity of the concrete specimens was observed in terms of age development, with a rapid increase between 7 days and 28 days, followed by slower growth at 56 days. It is because the resistivity was related to the porosity of the specimens and the concentration of ions in the water. When the age of the specimens was 7 days, the internal pores were large and the internal electron conduction was mainly carried out by ions such as Ca^{2+}, Na^{+}, K^{+}, OH^{-}, and SO_4^{2-} in the pore water, so the resistance coefficient was lower than that of the specimen at later age [26]. As the age increased, the internal pores gradually decreased. As a result of the hydration reaction, most of the ions are reacted, resulting in a significant reduction in conductivity. At this point, graphite in the specimens began to act as the main bridge between the electrons. This conclusion was consistent with previous research findings by Lee et al. [23] and Le et al. [41]. The addition of conductive powders could reduce the resistivity of the sensing concrete. When the addition amount reached the critical filler value (8% carbon black) [26], that is, the percolation threshold was reached, the trend of resistance reduction began to slow down [42].

3.8. Resistivity coefficient obtained using direct current (DC) loop resistance test

Figure 14 presents the resistivity coefficients derived using the DC loop resistance test. As can be seen in Figure 14(A), the normal concrete specimens with 4%, 8%, 12%, and 16% graphite contents show resistivity lower than that of the control group by 40.7%, 53.7%, 61.1%, and 64.8%, respectively. In Figure 14(B), the fiber specimens with 4%, 8%, 12%, and 16% graphite contents show resistivity reduction of 39.3%, 65.6%, 70.5%, and 75.4%, respectively.

The results indicate that the resistivity of the concrete dropped significantly with a 4% graphite content. When the graphite content was 8%, it declined by another 20%. Adding more graphite decreased the resistivity further, which gradually stabilized. The results show resistivity beginning to stabilize when the graphite content was between 8% and 16%, which means that an 8% graphite content is the percolation threshold of the concrete. Although the resistivity of the concrete dropped significantly with a 4% graphite content, it declined even more significantly as more graphite was added. It means that a 4% graphite content has not reached the percolation value of the concrete yet. The results of the pressure sensitivity test support these results.

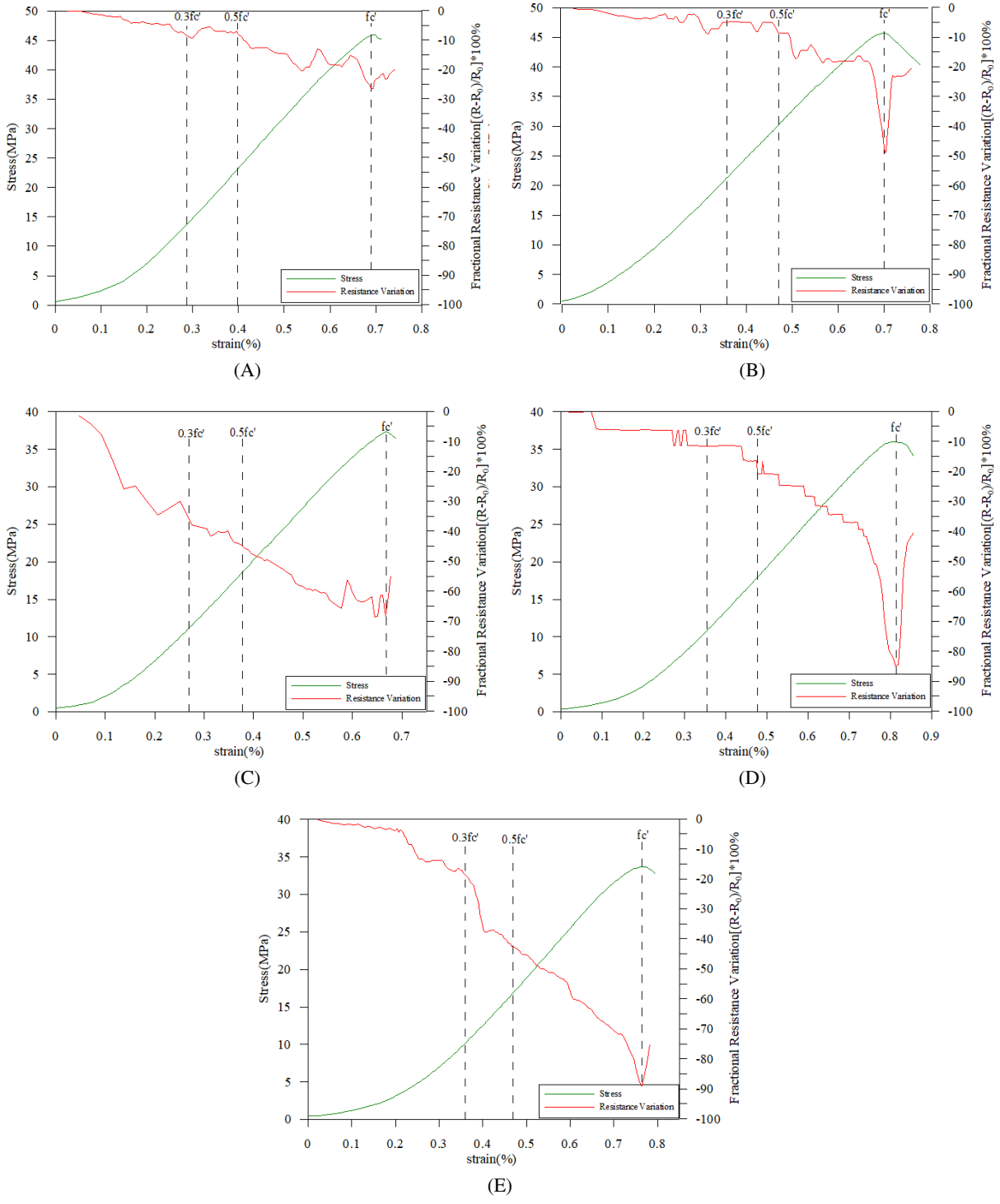


Fig. 15. Relationship between resistance variation, stress, and strain of the normal concrete group. **(A)** NG0, **(B)** NG4, **(C)** NG8, **(D)** NG12, and **(E)** NG16

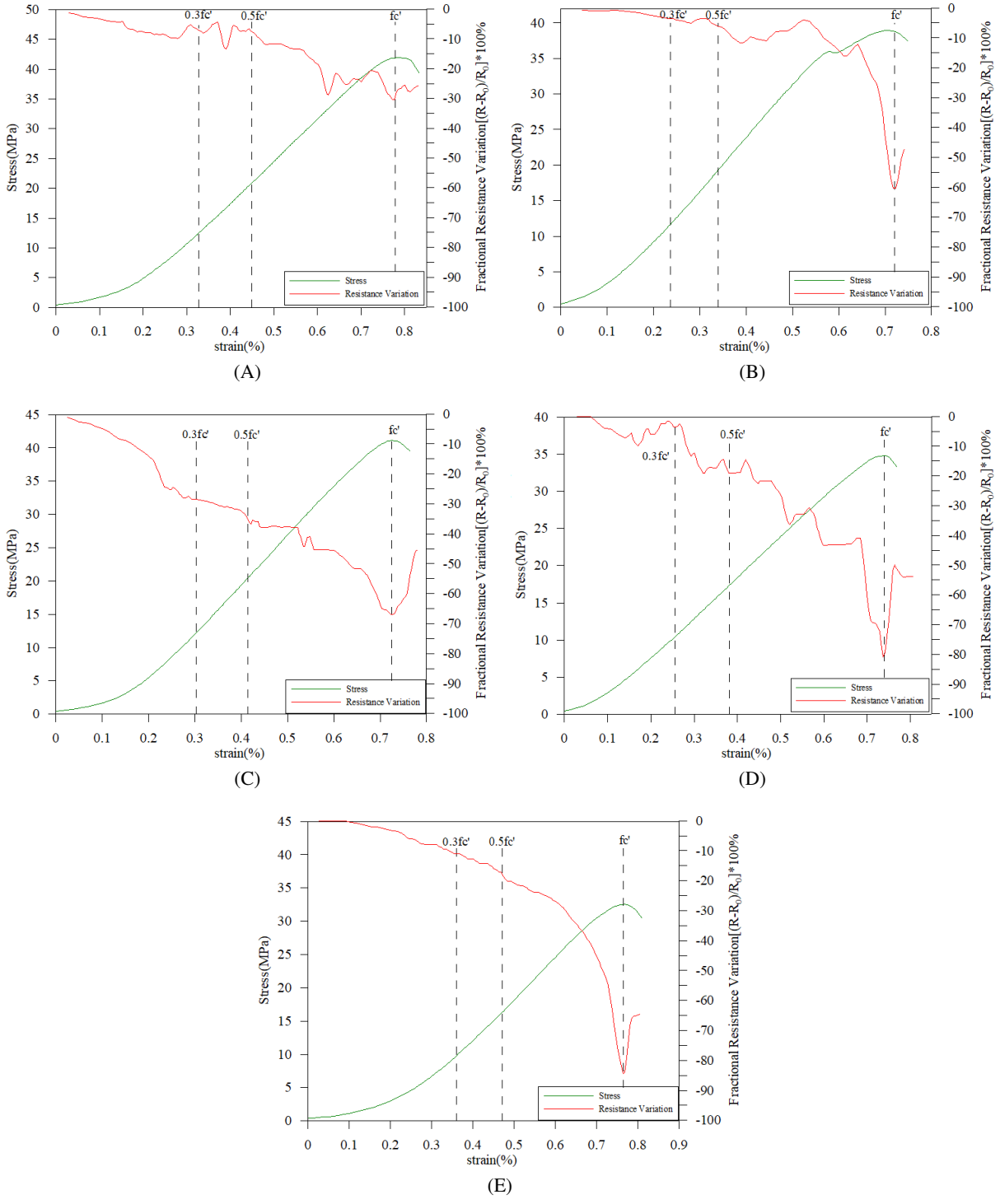


Fig. 16. Relationship between resistance variation, stress, and strain of the fiber concrete group. **(A)** KG0, **(B)** KG4, **(C)** KG8, **(D)** KG12, and **(E)** KG16

3.9. Relationship among resistance variation, stress, and strain

Figures 15 and 16 display the relationships among resistance variation, stress, and strain in the normal and fiber concrete specimens during the compressive strength tests. As can be seen, the normal and fiber concrete specimens containing no graphite presented poorer regularity as the load increased. During the earlier phase, the resistivity declined slightly. However, as the load increased and reached the fracture strength, the resistivity remained volatile and could not properly reflect the damage conditions within the specimens. The two normal and fiber concrete specimens with a 4% graphite content displayed similar circumstances in the earlier phase, with resistivity showing a significant decrease right before failure. Although the resistance variations in these two specimens were more apparent than those in the two specimens with no graphite, the percolation threshold was not reached. The two normal and fiber concrete specimens with an 8% graphite content also exhibited a considerable decline as the load increased; when the stress reached 50% of the ultimate load, the resistivity decreased less until failure, at which point the magnitude of the decline in the resistivity increased again. It indicates that the specimens have reached the percolation threshold. The normal and fiber concrete specimens with 12% and 16% graphite content showed similar trends in resistance variation, and resistivity decreased as stress increased until failure.

In terms of the range of variation in resistivity, the maximum variation ranged from 25% to 35% in the specimens with no graphite, from 50% to 60% in the specimens with a 4% graphite content, around 70% in the specimens with an 8% graphite content, from 80% to 85% in the specimens with a 12% graphite content, and from 85% to 90% in the specimens with a 16% graphite content. The greater variations in resistivity indicate that the specimens containing graphite formed better conductive networks during the compression process. These conductive powders (graphite) increased the sensitivity [43] and repeatability of the sensing concrete [44]. There was no significant difference in the electrical conductivity of the addition of fibers to sensing concrete. The fiber group had better sensitivity when the fiber concrete contained a low amount of graphite (4%).

Under uniaxial compression testing, the distance between conductive particles within the specimen was reduced, improving the conductive network within the concrete; when larger cracks appeared in the compressed specimen, the extension of the cracks led to the destruction of the conductive network. Although not significantly contributing to the conductivity, the addition of fibers was effective in mitigating damage to the conductive network caused by the extension of cracks. The test results also showed that the recovery rate of resistance variation was higher than that of the normal concrete group when the specimens exceeded the compressive failure strength, which is consistent with previous studies by Ding et al. [26] and Bekzhanova et al. [27].

3.10. Resistance variation during cyclic loading test

According to the study [40], fine cracks exist within most concrete materials. When the stress in the concrete equals 0%–30% of the ultimate load, the concrete is linear, and the fine cracks within do not develop. When the load applied to the concrete reaches 30%–40% of the ultimate load, the fine cracks begin to spread and increase with stress. At 70% of the ultimate load, visible cracks start to appear inside and on the surface of the concrete and worsen until failure.

Figure 17 presents the changes in resistivity in the ordinary specimens under cyclic loading at 50% of the ultimate load. When the control group specimen is in the linear phase, resistance variations are minor (10%) and do not exhibit clear correspondence to the changes in loading. The resistance variations in the concrete specimen with a 4% graphite content somewhat increase during the linear phase, ranging from 10% to 15%, but still show no apparent correspondence to the changes in loading. By contrast, the maximum resistance variations in the ordinary concrete specimens with 8% and 16% graphite contents range from 20% to 25%

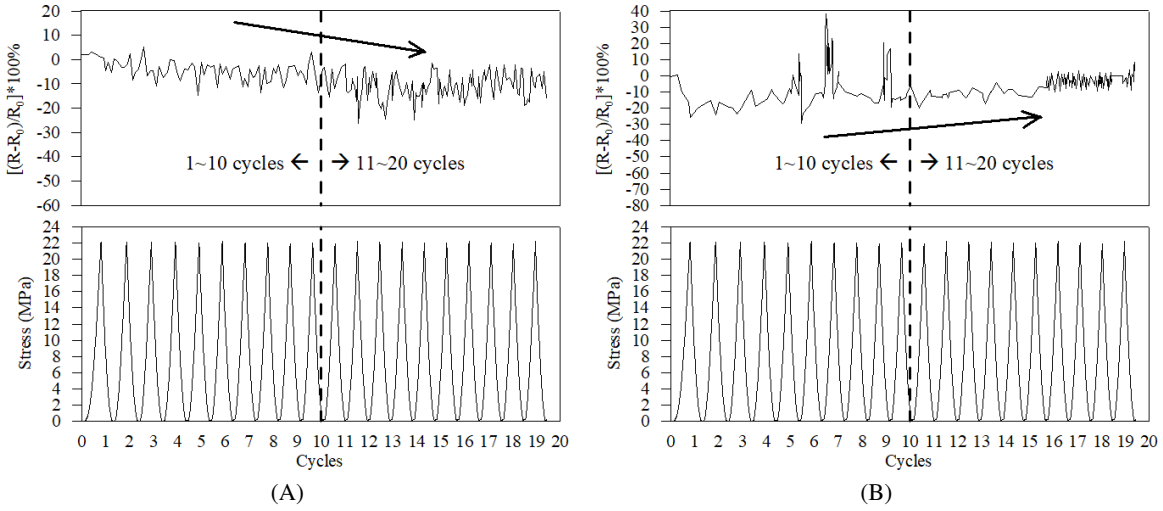


Fig. 17. Resistance variations in the normal specimens under cyclic loading at 50% of ultimate load. **(A)** NG0 specimens at 50% of the ultimate load, **(B)** NG4 specimens at 50% of the ultimate load, **(C)** NG8 specimens at 50% of the ultimate load, and **(D)** NG16 specimens at 50% of the ultimate load

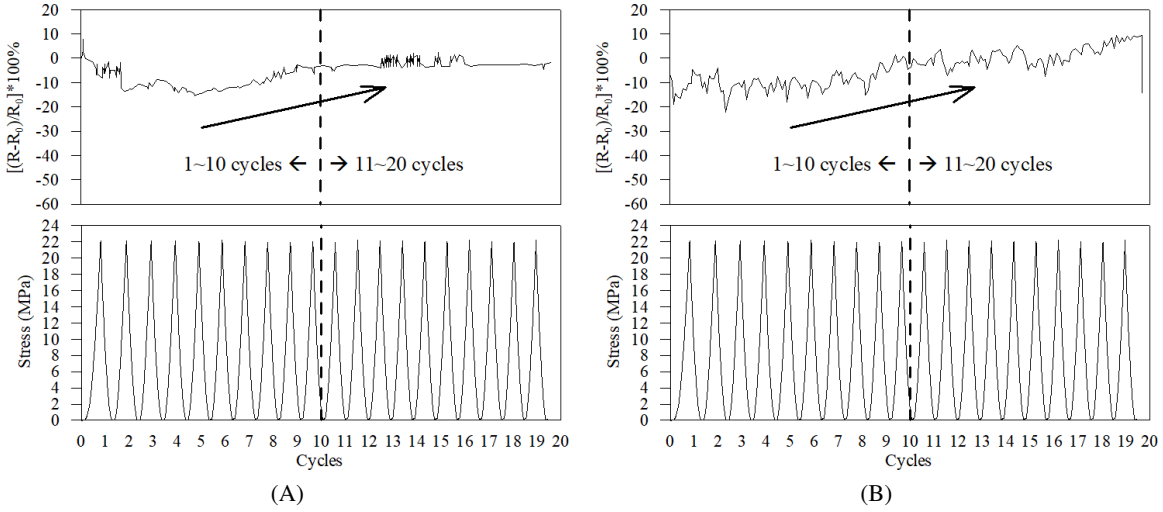


Fig. 18. Resistance variations in the fiber specimens under cyclic loading at 30% and 50% of ultimate load. **(A)** KG0 specimens at 50% of the ultimate load, **(B)** KG4 specimens at 50% of the ultimate load, **(C)** KG8 specimens at 50% of the ultimate load, and **(D)** KG16 specimens at 50% of the ultimate load

and show clear reactions to the changes in loading. Adding graphite powders to micro-scale secondary fillers effectively controlled the sensing performance of the sensing concrete, thereby increasing the maximum resistance variation and sensing sensitivity range when subjected to load.

Figure 18 presents the changes in resistivity in the fiber specimens under cyclic loading at 50% of the ultimate load. When the specimen containing no graphite is in the nonlinear phase, the resistance variations range from 15% to 25% and do not exhibit clear correspondence to the changes in loading. The resistance variations in the concrete specimen with a 4% graphite content range from 20% to 30% but still show no noticeable correspondence to the changes in loading like in the linear phase. By

contrast, the maximum resistance variations in the specimens with 8%, 12%, and 16% graphite content range from 30% and 40%, from 40% to 50%, and from 50% to 60%, respectively, and show clear reactions to the changes in loading. The test results show that the concrete specimens with a 8% graphite content or more present clearer resistance variations in the linear phase.

Excluding the specimens containing no graphite, whose resistance variations were too slight, only the resistivity of the specimens with a 4% graphite content could not return to their initial values. It speculated that the 4% graphite content was insufficient to form a complete conductive network in the specimens. Although loading reduced the pores within the concrete and enabled graphite particles to come into contact with one another, reducing the resistivity, the pores could not return to their original state upon unloading, thereby producing this result. Despite the pores being unable to return to their original condition in specimens with a higher graphite content, the better conductive networks in the concrete enabled resistivity to return to its initial value.

According to Mindess et al. [45], numerous cracks begin to form in specimens when subjected to loading at 40% of the ultimate strength. Comparing the specimens in the nonlinear phase revealed that resistivity presented slight increases with greater cycles. This phenomenon is most apparent in specimens NG8 and KG16. The increase in resistivity is possible because of the damage inflicted on the specimens during each loading process. In the form of minor cracks, the damage affected the conductive network within the specimens, causing the resistivity to increase with each loading irreversibly. The difference between normal and fiber concrete specimens can be seen in the specimens with 8% and 12% graphite concrete. After different loading processes, the normal concrete specimens show significant increases in resistivity. By contrast, the rising trend is not apparent in the resistivity of the fiber concrete specimens. It shows that adding K fibers to conductive concrete can reduce the speed at which cracks develop within concrete. The use of fibers can significantly reduce the trend of increasing resistivity [27] and has great potential for monitoring fatigue damage in different concrete structures [46].

4. Conclusion

The findings of mechanical properties show that the inclusion of graphite damages the mechanical properties and density of concrete, and the extent of damage increases with the graphite content. The inclusion of K fibers can increase the elastic and rupture moduli of the concrete. Furthermore, specimens with higher graphite contents display more significant differences in porosity than the control group as age progresses, which indicates that graphite and cement do not undergo hydration and should be classified as filling materials. Also, the inclusion of K fibers does not reduce concrete porosity significantly. According to the resistivity measurements from the four-electrode method and the DC loop resistance test, the lower bound of self-sensing properties in concrete is used as a content of 8% graphite.

The SEM images show that a 4% graphite content is sufficient to form an excellent conductive network. Once the graphite content reaches 12%, the graphite particles show clustering, but not conductivity. Concrete specimens reaching the percolation value showed good correspondence between loading and resistivity during the compressive strength test. Furthermore, the magnitude of resistance variations increased with the graphite content. During the cyclic loading tests at 50% of the ultimate load, the specimens with $>8\%$ graphite content showed good correspondence between loading and resistivity in the linear stage. The specimens with 8% and 12% graphite contents also showed increasing resistivity in the nonlinear phase as the number of cycles increased, demonstrating that these two graphite contents result in greater sensitivity to cracking.

The fiber specimens with 8% and 12% graphite contents did not show increasing resistivity as the number of cycles increased in the cyclic loading test, which means that the fibers can effectively prevent cracks within the specimens from connecting and increasing resistivity. The results show that in terms of strength requirements in en-

gineering, the specimen KG8 is the optimal mixture, which provides good sensitivity to pressure without damaging the mechanical properties significantly. This self-sensing concrete can be used in engineering cases such as bridges, concrete pavements, or building components. This self-sensing concrete offers better continuous monitoring and lower construction costs than traditional embedded sensors.

Acknowledgements

This research was supported by the National Science and Technology Council (NSTC) in Taiwan under the project No. 111-2923-E-197-001-MY3 and the Czech Science Foundation under the project No. 21-09922J.

References

[1] Chung DDL. Cement-matrix composites for smart structures. Smart Mater Struct. 2000;9:389–401.

[2] Chung DDL. Carbon materials for structural self-sensing, electromagnetic shielding and thermal interfacing. Carbon. 2012;50(9):3342–53.

[3] Ding Y, Chen Z, Han Z, Zhang Y, Pacheco-Torgal F. Nano-carbon black and carbon fiber as conductive materials for the diagnosing of the damage of concrete beam. Constr Build Mater. 2013;43:233–41.

[4] Gomis J, Galao O, Gomis V, Zornoza E, Garcés P. Self-heating and deicing conductive cement. Experimental study and modeling. Constr Build Mater. 2015;75:442–9.

[5] Ding Y, Huang Y, Zhang Y, Jalali S, Aguiar JB. Self-monitoring of freeze-thaw damage using triphasic electric conductive concrete. Constr Build Mater. 2015;101:440–6.

[6] Galao Y, Bañón L, Baeza F, Carmona J, Garcés P, Baeza JF. Highly conductive carbon fiber reinforced concrete for icing prevention and curing. Materials. 2016;9(4):281.

[7] Kočí V, Petříková M, Fořt J, Fiala L, Černý R. Preparation of self-heating alkali-activated materials using industrial waste products. J Clean Prod. 2020;260:121116.

[8] Carmona J, Garcés P, Climent MA. Efficiency of a conductive cement-based anodic system for the application of cathodic protection, cathodic prevention and electrochemical chloride extraction to control corrosion in reinforced concrete structures. Corros Sci. 2015;96:102–11.

[9] Cañón A, Garcés P, Climent MA, Carmona J, Zornoza E. Feasibility of electrochemical chloride extraction from structural reinforced concrete using a sprayed conductive graphite powder-cement paste as anode. Corros Sci. 2013;77:128–34.

[10] Trana YT, Lee J, Kumar P, Kim KH, Lee SS. Natural zeolite and its application in concrete composite production. Compos Part B-Eng. 2019;165(15):354–64.

[11] Markiv T, Sobol K, Franus M, Franus W. Mechanical and durability properties of concretes incorporating natural zeolite. Arch Civ Mech Eng. 2016;16(4):554–62.

[12] Gao JM, Sun W, Morino K. Mechanical properties of steel fiber-reinforced, high-strength, lightweight concrete. Cem Concr Comp. 1997;19(4):307–13.

[13] Iqbal S, Ali A, Holschemacher K. Mechanical properties of steel fiber reinforced high strength lightweight self-compacting concrete (shlscc). Constr Build Mater. 2015;98:325–33.

[14] Smirnova O, Kharitonov A, Belentsov Y. Influence of polyolefin fibers on the strength and deformability properties of road pavement concrete. J TrafficTransp Eng (Engl Ed). 2019;6(4):407–17.

[15] Abaeian R, Behbahani HP, Moslem SJ. Effects of high temperatures on mechanical behavior of high strength concrete reinforced with high performance synthetic macro polypropylene (HPP) fibres. Constr Build Mater. 2018;165:631–8.

[16] Fiala L, Rovnanik P, Černy R. Investigation of the Joule's effect in electrically enhanced alkali-activated aluminosilicates. Cement Wapno Beton. 2017;22(3):201–10.

[17] Rovnanik P, Kusak I, Bayer P, Schmid P, Fiala L. Comparison of electrical and self-sensing properties of Portland cement and alkali-activated slag mortars. Cem Concr Res. 2019;118:84–91.

[18] Yoo DY, Kim S, Lee SH. Self-sensing capability of ultra-high-performance concrete containing steel fibers and carbon nanotubes under tension. Sens Actuators A Phys. 2018;276:125–36.

[19] Chung DDL. Piezoresistive cement-matrixd materials for strain sensing. J Intell Mater Syst Struct. 2002;13:599–609.

[20] Gao J, Wang Z, Zhang T, Zhou L. Dispersion of carbon fibers in cement-based composites with different mixing methods. Constr Build Mater. 2017;134:220–7.

[21] Han B, Ding S, Yu X. Intrinsic self-sensing concrete and structures: a review. Measurement. 2015;59:110–28.

[22] Han B, Yu X, Kwon E. A self-sensing carbon nanotube/cement composite for traffic monitoring. Nanotechnology. 2009;20(44):445501.

[23] Lee SY, Le HV, Kim DJ. Self-stress sensing smart concrete containing fine steel slag aggregates and steel fibers under high compressive stress. Constr Build Mater. 2019;220:149–60.

[24] Dong W, Wang K, Luo Z, Sheng D. Self-sensing capabilities of cement-based sensor with layer-distributed conductive rubber fibres. Sens Actuators A Phys. 2020;301:111763.

[25] Sassani A, Arabzadeh A, Ceylan H, Kim S, Sadati SS, Gopalakrishnan K, et al. Carbon fiber-based electrically conductive concrete for salt-free deicing of pavements. J Clean Prod. 2018;203:799–809.

[26] Ding S, Dong S, Ashour A, Han B. Development of sensing concrete: principles, properties and its applications. Int J Appl Phys. 2019;126:241101.

[27] Bekzhanova Z, Memon SA, Kim JR. Self-sensing cementitious composites: review and perspective. Nanomaterials. 2021;11:2355.

[28] Teomete E. The effect of temperature and moisture on electrical resistance, strain sensitivity and crack sensitivity of steel fiber reinforced smart cement composite. Smart Mater Struct. 2016;25:075024.

[29] Demircilioğlu E, Teomete E, Schlangen E, Baeza FJ. Temperature and moisture effects on electrical resistance and strain sensitivity of smart concrete. Constr Build Mater. 2019;224:420–7.

[30] Hanxun B, Yu X, Zhang K, Kwon E, Ou J. Sensing properties of CNT-filled cement-based stress sensors. J Civ Struct Health Monit. 2011;1:17–24.

[31] Chen M, Gao P, Geng F, Zhang L, Liu H. Mechanical and smart properties of carbon fiber and graphite conductive concrete for internal damage monitoring of structure. Constr Build Mater. 2017;142:320–7.

[32] Fiala L, Toman J, Vodička J, Ráček V. Experimental study on electrical properties of steel-fibre reinforced concrete. Procedia Eng. 2016;151:241–8.

[33] Allam H, Duplan F, Amziane S, Burtschell Y. About the self-sensing behavior of smart concrete and its interaction with the carbon fiber percolation status, sand connectivity status and grain size distribution. Constr Build Mater. 2022;324:126609.

[34] Ding Y, Liu G, Hussain A, Pacheco-Torgal F, Zhang Y. Effect of steel fiber and carbon black on the self-sensing ability of concrete cracks under bending. Constr Build Mater. 2019;207:630–9.

[35] Cordon HCF, Tadini FB, Akiyama GA, de Andrade VO, da Silva RC. Development of electrically conductive concrete. Cerâmica. 2020;66:88–92.

[36] Wang B, Jiang R, Wu Z. Investigation of the mechanical properties and microstructure of graphene nanoplatelet-cement composite. Nanomaterials. 2016;6(11):200.

[37] Yang H, Cui H, Tang W, Li Z, Han N, Xing F. A critical review on research progress of graphene/cement based composites. Compos Part A: Appl Sci Manuf. 2017;102:273–96.

[38] Wang B, Pang B. Mechanical property and toughening mechanism of water reducing agents modified graphene nanoplatelets reinforced cement composites. Constr Build Mater. 2019;226:699–711.

[39] Kumar R, Bhattacharjee B. Assessment of permeation quality of concrete through mercury intrusion porosimetry. Cem Concr Res. 2004;34(2):321–8.

[40] Cheng A. Application of pressure-sensitive materials in cement-based composites for self-assessment of structural degradation. Asian J Chem. 2014;26(17):5691–8.

[41] Le HV, Kim MK, Kim SU, Chung SY, Kim DJ. Enhancing self-stress sensing ability of smart ultra-high performance concretes under compression by using nano functional fillers. J Build Eng. 2021;44:102717.

[42] Singh AP, Gupta BK, Mishra M, Chandra A, Mathur RB, Dhawan SK. Multiwalled carbon nanotube/cement composites with exceptional electromagnetic interference shielding properties. Carbon. 2013;56:86–96.

[43] Ding Y, Han Z, Zhang Y, Aguiar JB. Concrete with triphasic conductive materials for self-monitoring of cracking development subjected to flexure. Compos Struct. 2016;138:184–91.

[44] Han B, Zhang L, Sun S, Yu X, Dong X, Wu T, et al. Electrostatic self-assembled carbon nanotube/nano carbon black composite fillers reinforced cement-based materials with multifunctionality. Compos Part A Appl Sci Manuf. 2015;79:103–15.

[45] Mindess S, Young JF, Darwin D. Concrete. Pearson, editor. 2nd ed. New Jersey: Prentice-Hall; 2003.

[46] Feng Q, Ou J. Self-sensing CFRP fabric for structural strengthening and damage detection of reinforced concrete structures. Sensors. 2018;18:4137.

Received 2022-05-11
Accepted 2022-08-07